2024 IEEE International Conference on Robotics and Automation (ICRA 2024)
May 13-17, 2024. Yokohama, Japan

Untethered Underwater Soft Robot with Thrust Vectoring

Robin Hall and Cagdas D. Onal †

***Abstract*—This paper introduces DRAGON: Deformable Robot for Agile Guided Observation and Navigation, a free-swimming deformable impeller-powered vectored underwater vehicle (VUV). A 3D-printed wave spring structure directs the water drawn through the center of the robot by an impeller, enabling it to move smoothly in different directions. The robot is designed to have a narrow cylindrical profile to lower drag and improve agility. It has a maximum recorded speed of 2.1 BL/s (body lengths per second) and a minimum cost of transport (COT) of 2.9. The robot has two degrees of freedom (DoFs) and is capable of performing a variety of maneuvers including a full circle with a radius of 0.23 m (1.4 BL) and a figure eight, which it completed in 4.98 s (72.3 °/s) and 10.74 s respectively. We operated the robot, untethered, in various environments to test the robustness of the design and analyze its motion and performance.**

I. Introduction

The ocean presents a complex and unique environment that is vastly unexplored. Only 10% of the ocean floor has been mapped, almost exclusively in shallow coastal regions with measurements taken by surface vessels [1]. Deep ocean exploration has expanded over the past fifty years with the advent of advanced robots that are capable of operating in such harsh conditions. Only with the use of autonomous underwater vehicles (AUVs) and remotely operated vehicles (ROVs) were scientists able to confirm the existence of hydrothermal vents, a discovery that has shaped our understanding of the origins of life [2], [3].

Propeller-powered underwater robots are one of the most ubiquitous designs used in oceanographic research. They utilize motors with attached propellers to affect vertical and horizontal movement. Several motors are used to achieve multiple DoFs and accurate position control [4], [5]. This method is most effective when the robot is being actively controlled or is in a complex environment.

In some cases, multiple motors and active control is unnecessary and inefficient. For long-term autonomous open-ocean research, scientists use gliders, a design that translates forward motion from vertical velocity by leveraging active buoyancy control and dive planes [6]. These robots travel along a saw-toothed path and while incapable of highly accurate and precise movement, can travel for thousands of kilometers with very low power consumption [7].

*This material is based upon work partially supported by the National Science Foundation (NSF) under Grant Nos. CMMI-1752195, DGE-1922761. Any opinions, findings, and conclusions or recommendations expressed in this material are those of the authors and do not necessarily reflect the views of the NSF.

†The authors are with the WPI Soft Robotics Laboratory, Robotics Engineering Department, Worcester Polytechnic Institute, MA 01609, USA. All correspondence should be addressed to Cagdas Onal cdonal@wpi.edu

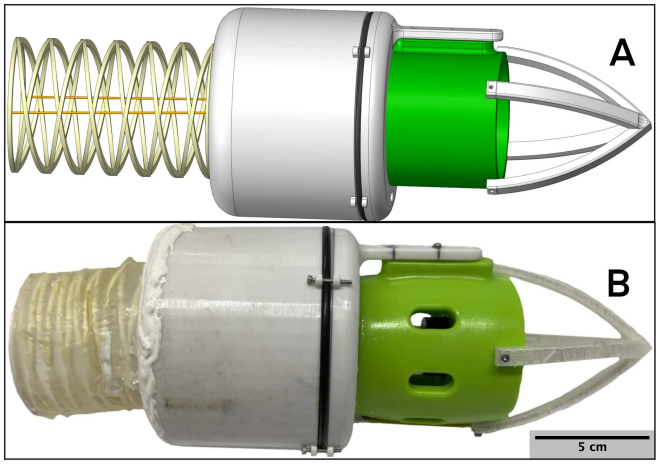

Fig. 1: (A) Cad model of the robot. (B) Physical robot with the addition of a latex skin on the wave spring tail. The skin combined with tension from the cables compressed the wave spring resulting in a difference in tail length compared (A). The robot's body length was 0.246 m.

Both styles of robots are complex and expensive to manufacture, costing anywhere between $50,000 to $5 million [8]. While more expensive robots are typically the most advanced, there is still a significant need to develop lower-cost high-performance robots to make robotics more accessible and usable in a wider range of work environments. Advances in additive manufacturing make it possible to quickly prototype robots using 3D printers and few materials.

Soft underwater robots also have the distinct advantage of being able to operate in environments that rigid robots cannot, like small caves or tight spaces. These robots are typically bio-inspired, minimizing their environmental impact, but are also inefficient. We merge the features of soft robots with the efficiency and speed benefits of propeller-driven rigid robots to introduce a unique soft robot.

We have developed a low-cost prototype VUV robot we call DRAGON (Deformable Robot for Agile Guided Observation and Navigation). DRAGON is printed from rigid and flexible materials and uses an impeller and active soft tail to swim. Unlike traditional propeller-powered robots that 'push' on water to move, this design uses a single impeller to draw water through the center of the robot and 'pull' itself forward. The active flexible tail helps direct the outflow of water; this eliminates the need for additional motors that increase cost and power consumption.

Our system (Fig. 1) is most analogous to a thrust vector propulsion system, like that of aircrafts or rockets. This provides a distinct advantage compared to traditional propeller systems. Standard designs rely on multiple fixed motors that

tilt the entire robot, potentially affecting the quality and accuracy of any sensors mounted to the body [9]. In contrast, vectored underwater vehicles (VUVs) can maintain a static body position while swimming. Our design also improves upon propeller-rudder control that is highly inefficient at low speeds [10].

There has been some prior work on modelling [10]–[13] and design [14]–[17] of VUVs. However, by leveraging both impeller-powered locomotion and a flexible tail, we have developed a robot that outperforms prior work and is capable of unmatched navigational agility at high speeds at a fraction of the cost of modern AUVs and ROVs.

The contributions of this work are as follows:

- The design and cost-effective fabrication of a deformable impeller robot.
- Efficient quantification of performance enabled by an untethered design.
- Comprehensive analysis of performance and maneuverability.

II. Design and Testing

The robot is operated by an impeller that pulls water through the center of the robot and the deformable wave spring tail. The wave spring can bend, directing the outflow of water, and thereby turning the robot. The robot is divided into three main parts: an impeller, servo motor and electronics housing, and a flexible tail.

A. Wave Spring Tail

The tail is a single cylindrical flexible wave spring fabricated by fused deposition modeling (FDM) using Ultimaker Thermoplastic Polyurethane (TPU) with a shore hardness of 95A. The structure is a mesh of diamond-shaped cells formed by two mirrored helices [18]. The wave spring can bend, stretch, compress, and is completely hollow. Water can pass through the center of the cylinder as well as the diamond-shaped cells. The wave spring is a versatile tool in underwater locomotion. More information on our use of wave springs for fish robots can be found in our prior work [19].

Since the wave spring is directing the outflow of water that is impelled through the robot, the hollow cells needed to be covered so water only exits the wave spring at the correct end. This was accomplished by the addition of a latex skin that was wrapped around the outside of the wave spring. The latex sealed the wave spring while not affecting its ability to bend.

One end of the wave spring is fixed to the body of the robot and the other end is connected internally by polyethylene non-elastic braided cables to a 20 kg-cm, 0.080 s per 60°-rated servo motor (Fig. 2). The cables are wound around a 4 mm diameter spool that is affixed to the servo motor. As the motor rotates from 90° to 0°, the wave spring bends left, and as the motor rotates from 90° to 180°, the wave spring bends right.

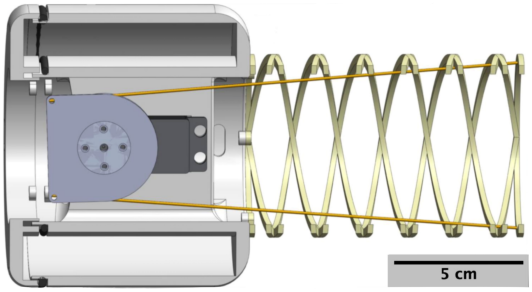

Fig. 2: Top view of electronics housing and wave spring tail CAD. The body is toroidal in shape to provide a dry compartment for electronics while maintaining a slim cylindrical body profile and a channel for water to pass through the robot.

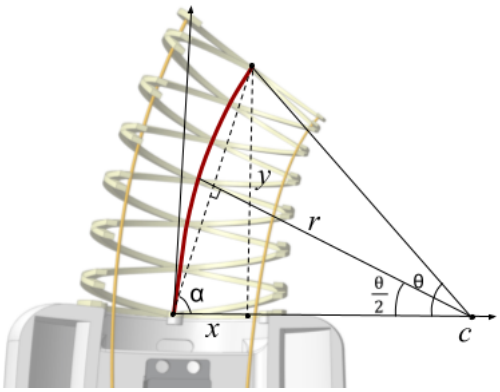

Fig. 3: The bending angle of the wave spring module is calculated assuming curvature along the curve (red) is constant. x and y are the coordinates at the tip of the wave spring, r is the radius of curvature of the curve, α is the angle between the x-axis and the hypotenuse of the right triangle generated by x and y, and θ is the bending angle calculated by Eq. 1 and 2.

Assuming constant curvature [20] and the measured positions of the bent body, we calculated the bending angle of the wave spring tail:

$$\alpha = cos^{-1}\frac{x}{\sqrt{x^2+y^2}}, \tag{1}$$

$$\theta = (\frac{\pi}{2} - \alpha)\frac{360}{\pi}, \tag{2}$$

where x and y are the coordinates of the center of the wave spring tip and α is the angle between the x-axis and the virtual line generated from the tip of the wave spring to the origin. α is shared by both triangles in Fig. 3, so using the law of cosines, we calculated the bending angle θ (Eq. 1 and 2). The maximum bending angle to the right was 25° and to the left was 31° (Fig. 4). This difference is likely due to wear on both the cables and wave spring.

B. Electronics Housing

The servo motor that bends the wave spring sits at the center of a toroidal-shaped container that houses the electronics that drive the robot. The torus shape is critical to the design of the robot as it provides a sealed compartment for electronics that cannot be exposed to water, while still allowing the flow of water to pass through the center.

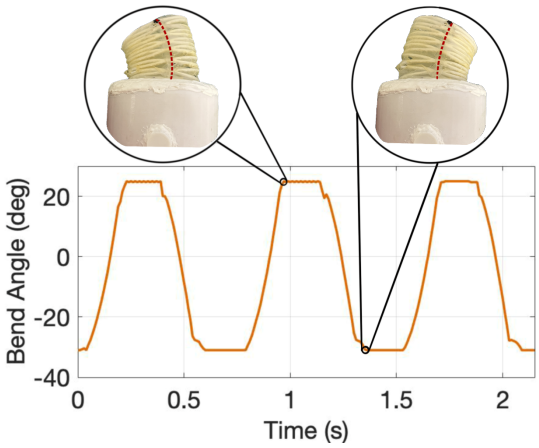

Fig. 4: Bending angle is represented by positive and negative integers corresponding to right and left bend direction respectively. A 0° bending angle corresponds to the robot moving in a straight line. Three cycles of bending are shown to demonstrate the rapid directional changes the robot is capable of. The tail fully changes direction in 0.2 s.

The robot is radio-controlled by an RFM9x Lora Radio module. A transponder module is powered by an Arduino Uno on land that sends signals to a receiver module on the robot. All functions on the robot are controlled by an Ardunio Nano on board, selected for its ease of use and small physical profile. The Arduino Nano controls the receiver module, servo motor, 30A Brushless electronic speed controller (ESC), and an INA219 Current Monitor used to collect power consumption data for cost of transport (COT) calculations. Each board, along with a 450 mAh lithium polymer battery, are stored inside the toroidal container. Once sealed, this container was positively buoyant, so a 160 g counterweight was added to achieve neutral buoyancy.

The servo motor actively moves the wave spring, placing it outside the electronics container and permanently exposing it to water. 3M 5200 flexible marine sealant was applied to all the seams along the body of the motor and a gasket with silicone grease was used to seal the servo horn. The spool rotated by the servo motor must also be centered to evenly bend the wave spring. Therefore, the dimensions of the servo motor and its spool dictated the minimum size of the container, resulting in a height of 0.1 m and a total body length of 0.246 m.

C. Impeller

DRAGON was designed to have as small of a profile as possible to enhance mobility in complex environments. The physical profile of the impeller, an off-the-shelf 600 kv motor designed for underwater applications, is a cylinder 65 mm in diameter and 70 mm in length. This defined the cylindrical shape of the rest of the robot; both the electronics container and the wave spring were designed to be cylindrical with an inner diameter of 65 mm. The outer diameter of the electronics container had to be wider, 100 mm in diameter, to account for the size of the battery and the ESC, the largest components that were stored.

One end of the impeller was affixed to the electronics housing to pull water through the center of the robot. The impeller is connected to a 30A Brushless ESC that is in turn connected to the Arduino Nano. The other end of the impeller forms the head of the robot. In initial testing, the robot's movement was impeded if the exposed end of the impeller came into contact with a flat surface, effectively sticking the robot to that surface. To mitigate this challenge, a teardrop-shaped nose was added to the exposed end of the impeller. This nose was a simple four-spoke design to provide a strong structure while remaining mostly hollow to not block water from entering the impeller.

During testing, we also found that when under power, the robot would dive forward instead of swimming straight, even if the whole system was statically neutrally buoyant, possibly due to small assembly errors affecting the thrust vector. To counteract this effect, closed-cell foam was added around the end of the impeller to increase buoyancy at the very end of the robot. This successfully prevented it from diving.

D. Radio Control Scheme

We decided to use simple radio control over more complicated methods like acoustics in order to expedite development. While acoustics will work better long-term and for deeper dives, radio signals functioned well in our three shallow testing environments.

As previously stated, the robot is controlled using long-range radio modules operating on two separate Arduino boards (Fig. 5). The transponder is housed in a small box on land, which protects the electronics in case of contact with water. Two potentiometers are used to control both the servo angle and the impeller speed. Readings from the potentiometers are transmitted to the receiver on the robot, which responds accordingly.

E. Performance Metrics and Experimentation

Several parameters were analyzed to quantify the performance of the robot including speed, COT, turning radius, and maneuverability. We evaluated the speed and COT of the robot swimming in a straight line. Speed is useful to compare our performance to other robots and COT is used to measure the efficiency of the robot under different conditions. COT is defined as:

$$COT = \frac{P}{mg\bar{v}}, \tag{3}$$

where $P = VI$ is the average power consumption, (V is the average voltage and I is the average current measured throughout the duration of the test), m is mass in kg, g is the acceleration due to gravity in m/s^2, and $\bar{v}$ is the average velocity of the robot over the duration of the test in m/s. The robot was run in the tank for 1 m and the speed was recorded using PHYSLETS TRACKER [21] while the power consumption was recorded using the onboard INA219 Current Monitor.

We quantified the maneuverability of the robot by measuring its turning radius while swimming in a complete circle

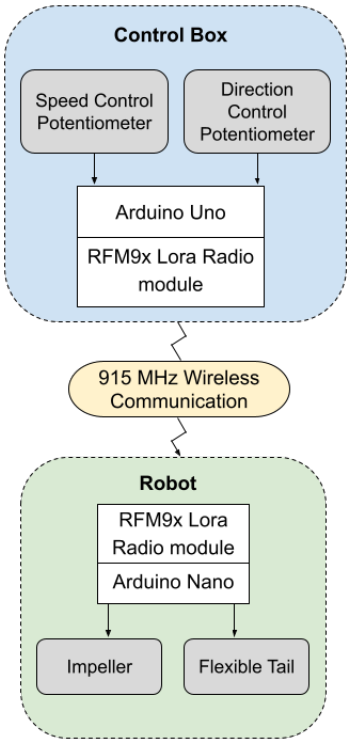

Fig. 5: Communication diagram illustrates the control scheme used to operate the robot. Two potentiometers are available to the user to change the speed and direction of the robot. Those commands are sent wirelessly via 915 MHz radio signals, and the impeller and flexible tail move accordingly.

as well as the time it took to complete the action. The robot also performed a figure-eight maneuver to demonstrate more advanced agility capabilities.

Initial testing took place in a 1.2x0.45x0.53 m fish tank filled roughly 80% with tap water. The robot needed more room to make full turns and reach its maximum speed, so additional data was collected from tests executed in Lake Quinsigamond in Worcester, Massachusetts and the Worcester Polytechnic Institute swimming pool. Tests were recorded and analyzed using PHYSLETS TRACKER [21].

III. RESULTS AND DISCUSSION

In summary, DRAGON can attain a maximum speed of 2.1 BL/s with a COT of 4.3. The minimum COT was 2.9 at 50% speed. The robot also completed a full circle with a radius of 1.4 BL in 4.98 s (72.3°/s) and a figure eight maneuver in 10.74 s.

A. Speed and COT

The robot's speed was recorded over several tests traveling in a straight line for 1 m. The average speed was 1.7 BL/s with a maximum speed of 2.1 BL/s. The robot was able to maintain high speeds while maneuvering.

Power consumption strongly correlated to the speed of the impeller and the servo motion simply addsed noise (Fig. 6). When the servo was in a fixed position, as it was for the COT tests, it had a negligible effect on the COT.

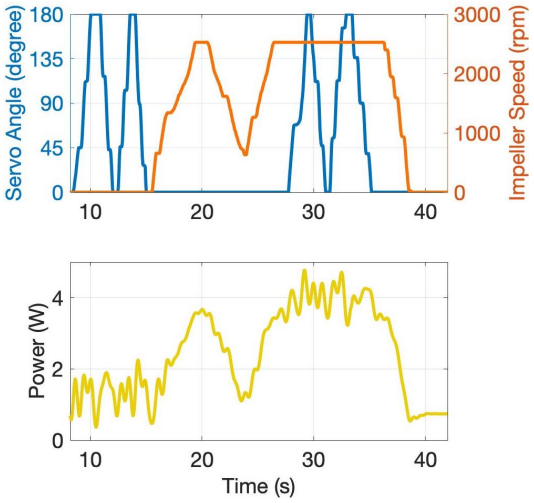

Fig. 6: Power consumption is directly related to the movement of both the impeller and flexible tail. From 0 - 15 s, the servo was sweeping between 0 and 180° while the impeller was not moving. From 15 - 17 s, the servo was at a fixed position while the impeller was sweeping between 0 and 2525 rpm, its maximum speed. Finally from 27 - 35 s, the impeller was operating at 2525 rpm while the servo was sweeping between 0 and 180°. Situations that require the robot to maneuver under high speeds consumes the most power, while constant cruising consumes very little power.

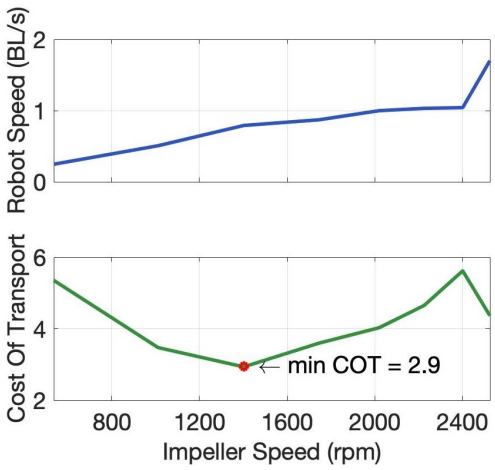

Fig. 7: Impeller speed was increased by 10% from 0 to 2525 rpm. The slowest impeller speed achievable was 535 rpm resulting in a speed of 0.25 BL/s. The lowest COT recorded was 2.9 at 1402 rpm when the robot was operating at 50% power and swimming 0.8 BL/s. At the robots average maximum speed of 1.7 BL/s, COT decreases to 4.3. It was evident that the significant increase in speed at 2525 rpm resulted in a commensurate decrease in COT. We will investigate using a more powerful impeller to see if this decrease in COT continues.

COT was measured by increasing impeller speed by 10% from 0 rpm to 2525 rpm (Fig. 7). The lowest COT recorded was 2.9 at 50% power (1402 rpm) and the highest was 5.6 at 90% (2401 rpm). The robot's top speed was at 100% power (2525 rpm) with a COT of 4.3. While this speed was not the most efficient, it was more than twice as fast as the robot at 50% power. These results provide us with a baseline for future work, where we will work to improve the efficiency

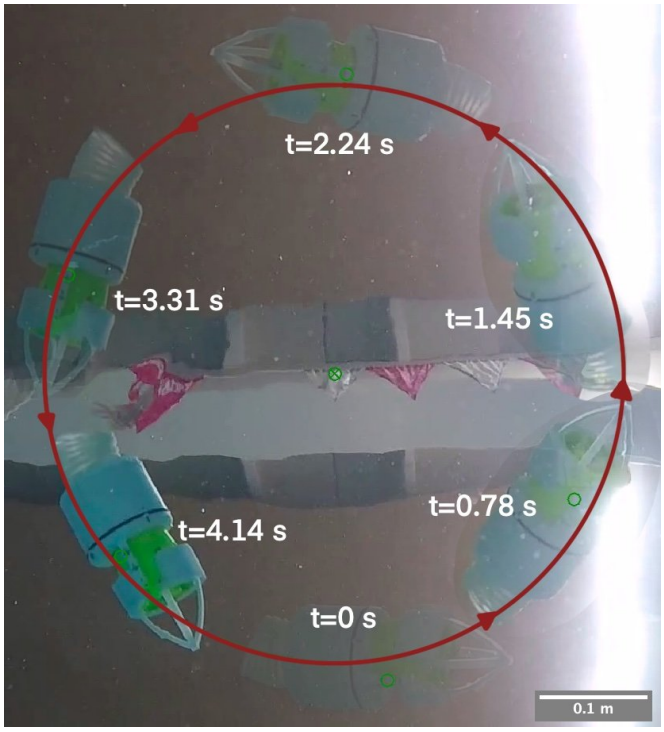

Fig. 8: The robot was moving counterclockwise in a circle that is 0.23 m (1.4 BL). Major time steps along the circle are shown in increasing opacity. The robot completed the circle in 4.98 s (72.3°/s).

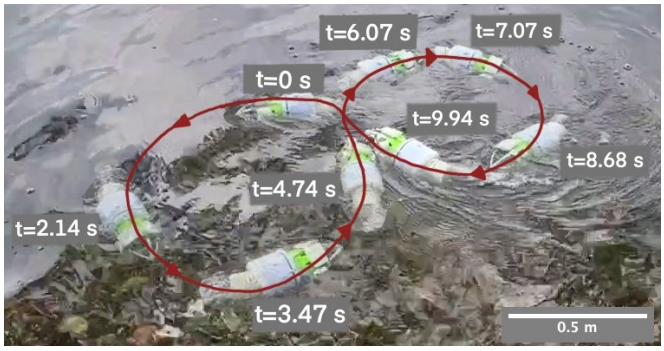

Fig. 9: The robot was actively controlled in a figure eight pattern. Major time steps along the path are shown to help illustrate the path the robot is traveling. It completed the maneuver in 10.74 s, roughly twice as long as it took to complete one circle.

of the robot while maintaining its maximum speed.

B. Maneuverability and Robustness

By placing a camera underneath the robot, we were able to capture data while the robot completed several circles (Fig. 8). The robot's minimum turning radius was 0.23 m (1.4 BL). The robot completed these circles in an average time of 4.98 s (72.3°/s). As the robot completed successive circles, it experienced some lateral drift. The robot shifted 24.8 mm from its starting location to its ending location after three circles.

To validate the agility of the robot, a figure eight maneuver was tested (Fig. 9). This was accomplished by maintaining a constant velocity and depth, while actively controlling the flexible tail. The robot completed the maneuver in 10.74 s, which is roughly double the time it took for the robot to complete a single circle.

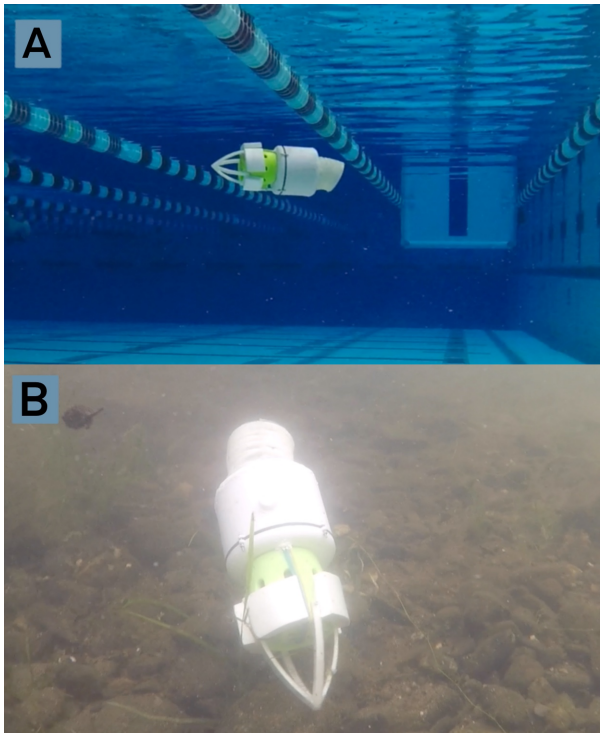

Fig. 10: (A) Robustness testing in Worcester Polytechnic Institute swimming pool and (B) Lake Quinsigamond. The robot was able to operate at depths of 0 m to 5 m in the pool and functioned with disturbances from wake and debris in the lake.

We tested the robot at various depths spanning from 0 m to 5 m in a swimming pool. The robot operated at full capacity at any depth but due to its lack of buoyancy control, it either floated to the surface or sank to the bottom over time. Actively controlling the buoyancy or adding the ability to move in three dimensions could help mitigate this issue. The robot was also tested in a lake environment to verify that it worked in a natural environment. The robot was able to swim at depths from 0 m to 2 m while generally unaffected by boat wakes or debris in the lake. The robot was able to maintain its heading despite occasional disturbances. After testing, debris like weeds and dirt had to be removed from the impeller motor. A method to prevent motor interference should be implemented. Snapshots from these tests are seen in Fig. 10 and footage from both environments can be seen in the reference video.

C. Performance Comparison

The agility of DRAGON depends on its length and especially the bending angle of the wave spring tail. The maximum right and left bending angle on the current design was 25° and 31° respectively. Increasing the bending angle and decreasing the length of the rigid portion of the robot would result in a smaller turning radius and increase the overall

TABLE I: Comparison with Various Underwater Robots and Biological Fish

Name and Source	Speed (BL/s)	Turning Radius (m)	Body Length (m)	Type	Propulsion Method	Untethered
Piezoceramic Fish Robot [22]	0.29	0.41	0.26	Soft	Undulation	No
Gliding Robotic Fish [23]	0.52	0.9	0.4	Rigid	Undulation	Yes
Wire-Driven Fish [24]	0.66	0.13	0.55	Soft	Undulation	Yes
Micro-robot fish [25]	0.75	0.14	0.15	Soft	Undulation	Yes
Two-Joint Fish [26]	0.77	1.76	1.76	Rigid	Undulation	Yes
Screw Propeller [26]	0.88	4	1.6	Rigid	Propeller	Yes
DRAGON	2.1	0.23	0.25	Soft	Impeller	Yes
MASUV-1 [17]	2.14	1.2	0.7	Rigid	Impeller	Yes
STARFISH AUV [27]	2.65	5.9	1.6	Rigid	Propeller	Yes
Cyprinus carpio koi [28]	1.5	0.03	0.06	Bio	Undulation	-
Ostracion cubicus [29]	5	0.001	0.1	Bio	Undulation	-

maneuverability of the robot. However, even the current prototype's maneuverability outperforms other biologically inspired or propeller-powered robots.

Biologically inspired robots modelled after fish (using a caudal tail for locomotion) tend to be less agile. Some [22], [23], [26] had a much larger turning radius while others [24], [25] had a smaller turning radius but operated up to twice as slow (Table I). Biologically inspired designs offer some advantages in scope, but ultimately can fall short when it comes to speed and maneuverability.

Propeller-powered robots are often larger and can deliver more power, making them on average faster. However, their larger size and lack of flexibility significantly reduces their agility, the closest comparison robot [17] in speed and size having a turning radius almost five times larger than DRAGON. Biological fish still have an advantage in terms of both turning radius and speed, which gives us a target to improve our design to perform comparably with biological counterparts.

We have created an agile and fast underwater vehicle that exhibits high speeds and maneuverability by combining elements of vector thrusting in an impeller-driven soft robotic body. It performs especially well compared to other soft underwater robots and is also untethered, often a challenge for soft robots that require complicated or heavy actuation systems. The combination of novel soft materials and traditional rigid motors makes this robot a unique and powerful design that opens up multiple applications. Additionally, the total manufacturing cost is generously estimated to be $140 USD, less than 0.5% the cost of some underwater vehicles on the market today. Even with the proposed design improvements, our use of off-the-shelf electronics and rapid additive manufacturing will ensure future versions of the robot cost to remain low. Without sacrificing performance, we are able to reduce costs with the goal of making robots ubiquitous in all facets of underwater research.

IV. Conclusion

This work presented DRAGON, a highly maneuverable and fast robot that leverages soft materials to enhance traditional robotic swimming methods. The robot has a maximum recorded speed of 2.1 BL/s and a minimum COT of 2.9. The robot is also able to execute circle and figure eight maneuvers with radii of 0.23 m (1.4-BL) in 4.98 s (72.3 °/s) and 10.74 s respectively. An impeller and flexible tail work in concert to create a two-DoF swimming robot operated using simple radio control.

The current design, while successful, was a proof-of-concept and there are several planned improvements that will be made to this system. The first priority will be increasing the degrees of freedom. We tested the robot's ability to swim in the vertical plane (rising and diving) by rotating the internal counter weight 90°. The robot is very capable of rising, aided by the fixed neutral buoyancy, but struggled to dive. The methods used to prevent the robot from uncontrolled diving in initial testing could be replaced by adding control over additional degrees of freedom.

Another major improvement will be implementing a communication framework better suited to underwater environments. The radio control modules had signal problems at 3 m when the robot was underwater. When the robot looses signal, it is programmed to repeat the last command indefinitely to not interfere with data collection. This is helpful for our current model, but we will look to implement a better failsafe for future situations where contact with the robot is lost. Acoustic communication methods have been shown to be effective for underwater robots and would be a critical improvement as the robot is operating at varied depths.

This robot is inexpensive and simple to manufacture compared to currently available underwater robots used for research purposes. Our motivation is to develop a robot that can be used by climate researchers to monitor and take action in complex environments like coral reefs that are greatly affected by rapidly changing ocean climates. Developing a highly dexterous, yet inexpensive, robot will be a valuable tool for scientists who are trying to better understand the dire impacts of climate change on sensitive ecosystems and species, especially in tight spaces that are inaccessible for existing underwater vehicles.

REFERENCES

[1] Matthew A. Charette and Walter H. F. Smith. The Volume of Earth's Ocean. *Oceanography*, 23(2):112–114, 2010.

[2] Jennifer B. Paduan, Robert A. Zierenberg, David A. Clague, Ronald M. Spelz, David W. Caress, Giancarlo Troni, Hans Thomas, Justin Glessner, Marvin D. Lilley, Thomas Lorenson, John Lupton, Florian Neumann, Miguel A. Santa Rosa-del Rio, and C. Geoffrey Wheat. Discovery of Hydrothermal Vent Fields on Alarcón Rise and in Southern Pescadero Basin, Gulf of California. *Geochemistry, Geophysics, Geosystems*, 19(12):4788–4819, 2018.

[3] Eva Ramirez-Llodra, Timothy M. Shank, and Christopher R. German. Biodiversity and Biogeography of Hydrothermal Vent Species: Thirty Years of Discovery and Investigations. *Oceanography*, 20(1):30–41, 2007.

[4] Mohd Shahrieel Mohd Aras, Hyreil Kasdirin, Muhammad Jamaluddin, and Md Basar. Design and Development of an Autonomous Underwater Vehicle (AUV-FKEUTeM). *Proceedings of MUCEET2009 Malaysian Technical Universities Conference on Engineering and Technology, MUCEET2009, MS Garden, Kuantan, Pahang, Malaysia*, January 2009.

[5] M. Dunbabin, J. Roberts, K. Usher, G. Winstanley, and P. Corke. A Hybrid AUV Design for Shallow Water Reef Navigation. In *Proceedings of the 2005 IEEE International Conference on Robotics and Automation*, pages 2105–2110, April 2005.

[6] Barkat Ullah, Mark Ovinis, Masri B Baharom, M. Y. Javaid, and S. S. Izhar. Underwater gliders control strategies: A review. In *2015 10th Asian Control Conference (ASCC)*, pages 1–6, May 2015.

[7] Stephen Wood and Alexander Inzartsev. Underwater Vehicles. pages 505–535, January 2009.

[8] Oscar Schofield, Scott Glenn, and Mark Moline. The Robot Ocean Network. *American Scientist*, 101(6):434, February 2017.

[9] Suiyang Khoo, Michael Norton, Jayanth Jaya Kumar, Juliang Yin, Xin Yu, Tim Macpherson, Denis Dowling, and Abbas Kouzani. Robust control of novel thrust vectored 3D printed multicopter. In *2017 36th Chinese Control Conference (CCC)*, pages 1270–1275, July 2017.

[10] Xiaoxu Du, Hang Cui, and Zhengdong Zhang. Dynamics model and maneuverability of a novel AUV with a deflectable duct propeller. *Ocean Engineering*, 163:191–206, September 2018.

[11] Rajat Mishra and Mandar Chitre. Modelling of an AUV with Voith-Schneider vector thruster. In *2016 IEEE/OES Autonomous Underwater Vehicles (AUV)*, pages 355–359, November 2016.

[12] Rongmin Zhang, Yuan Chen, Jun Gao, and School of Mechanical, Electrical & Information Engineering, Shandong University at Weihai. Numerical Investigation on Transverse Maneuverability of a Vectored Underwater Vehicle Without Appendage. *Journal of Robotics and Mechatronics*, 28(3):371–377, June 2016.

[13] Tao Liu, Yuli Hu, and Hui Xu. Deep Reinforcement Learning for Vectored Thruster Autonomous Underwater Vehicle Control. *Complexity*, 2021:e6649625, April 2021.

[14] Ba Xin, Luo Xiaohui, Shi Zhaocun, and Zhu Yuquan. A vectored water jet propulsion method for autonomous underwater vehicles. *Ocean Engineering*, 74:133–140, December 2013.

[15] Yansheng Li, Meimei Yang, Hanxu Sun, Zhimin Liu, and Yi Zhang. A Novel Amphibious Spherical Robot Equipped with Flywheel, Pendulum, and Propeller. *Journal of Intelligent & Robotic Systems*, 89(3):485–501, March 2018.

[16] Shuxiang Guo, Xichuan Lin, Koujirou Tanaka, and Seji Hata. Development and control of a vectored water-jet-based spherical underwater vehicle. In *The 2010 IEEE International Conference on Information and Automation*, pages 1341–1346, June 2010.

[17] Vladislav Kopman, Nicholas Cavaliere, and Maurizio Porfiri. MASUV-1: A Miniature Underwater Vehicle With Multidirectional Thrust Vectoring for Safe Animal Interactions. *IEEE/ASME Transactions on Mechatronics*, 17(3):563–571, June 2012.

[18] Erik H. Skorina and Cagdas D. Onal. Soft Hybrid Wave Spring Actuators. *Advanced Intelligent Systems*, 2(1):1900097, 2020.

[19] Robin Hall and Erik Skorina. The Effect of Design and Control Parameters of a Soft Robotic Fish Tail to Maximize Propulsion Force in Undulatory Actuation. *RAS/EMBS IEEE 9th International Conference on Biomedical Robotics and Biomechatronics*, January 2022.

[20] Shou-Shan Chiang, Hao Yang, Erik Skorina, and Cagdas D. Onal. SLInKi: State Lattice based Inverse Kinematics - A Fast, Accurate, and Flexible IK Solver for Soft Continuum Robot Manipulators. In *2021 IEEE 17th International Conference on Automation Science and Engineering (CASE)*, pages 1871–1877, August 2021.

[21] Douglas Brown, Christian Wolfgang, and Robert. Hanson. Tracker Video Analysis and Modeling Tool for Physics Education. https://physlets.org/tracker/, 2023.

[22] Q. S. Nguyen, S. Heo, H. C. Park, and D. Byun. Performance evaluation of an improved fish robot actuated by piezoceramic actuators. *Smart Materials and Structures*, 19(3):035030, February 2010.

[23] Feitian Zhang, Fumin Zhang, and Xiaobo Tan. Steady spiraling motion of gliding robotic fish. In *2012 IEEE/RSJ International Conference on Intelligent Robots and Systems*, pages 1754–1759, October 2012.

[24] Yong Zhong, Zheng Li, and Ruxu Du. The design and prototyping of a wire-driven robot fish with pectoral fins. In *2013 IEEE International Conference on Robotics and Biomimetics (ROBIO)*, pages 1918–1923, December 2013.

[25] Zhenlong Wang, Guanrong Hang, Jian Li, Yangwei Wang, and Kai Xiao. A micro-robot fish with embedded SMA wire actuated flexible biomimetic fin. *Sensors and Actuators A: Physical*, 144(2):354–360, June 2008.

[26] Jianhong Liang, Tianmiao Wang, and Li Wen. Development of a two-joint robotic fish for real-world exploration. *Journal of Field Robotics*, 28(1):70–79, 2011.

[27] You Eng, Kwong Meng Teo, Mandar Chitre, and Kien Ng. Online System Identification of an Autonomous Underwater Vehicle Via In-Field Experiments. *IEEE Journal of Oceanic Engineering*, 41:1–1, March 2015.

[28] Guanhao Wu, Yan Yang, and Lijiang Zeng. Routine turning maneuvers of koi carp Cyprinus carpio koi:effects of turning rate on kinematics and hydrodynamics. *Journal of Experimental Biology*, 210(24):4379–4389, December 2007.

[29] Jeffrey Walker. Kinematics and Performance of Maneuvering Control Surfaces in Teleost Fishes. *Oceanic Engineering, IEEE Journal of*, 29:572–584, August 2004.